Structure and energetics of Xe_n^-: Many-body polarization effects

Glenn J. Martyna and Bruce J. Berne
Department of Chemistry, Columbia University, New York, New York 10027

(Received 13 September 1988; accepted 2 December 1988)

In a previous paper, Martyna and Berne, J. Chem. Phys. **88**, 4516 (1988), diffusion Monte Carlo simulations were performed to determine the absolute binding energies of an excess electron to small clusters of xenon atoms ($n \leqslant 19$) using a pair additive pseudopotential. In this approximation, the electron–xenon polarization energy is treated as pair additive and therefore ignores the induced dipole–induced dipole interactions. Here we treat the many-body polarization problem in the dipole approximation. It is found that while the smallest stable cluster anion is Xe_6^- for the pair polarization model this increases to Xe_7^- for the many-body polarization model. In fact, the electron binding energy corresponding to the pair-polarization model was found to be a factor of 2.7 larger than for the many-body polarization model for all the clusters studied. In accord with this very large destabilization of electron binding energy (induced by many-body polarization), the spatial extent of the electronic ground state in the many-body polarization model increases compared to that of the pair polarization model. We also compare our results for both the many-body polarization and the two-body polarization models to corresponding dielectric continuum models developed by Stampfli and Bennemann, Phys. Rev. A **71**, 1674 (1988). In the many-body polarization case, the continuum model agrees well with our results. However, the agreement in the pair polarization case is rather poor for all cluster sizes. If parameters of the continuum model are adjusted to obtain agreement for small clusters sizes, the model is found to break down for large clusters sizes where the spatial extent of the electron is small enough that the microscopic details of the cluster become extremely important. A new variant of the fast Fourier transform projector method suitable for use in problems involving electron attachment to clusters is also developed. The results obtained with this new method are shown to agree with those of diffusion Monte Carlo.

I. INTRODUCTION

Recently we have studied the electron binding energy and structure of xenon cluster anions Xe_n^-,[1] where the electron was assumed to interact with each of the xenon atoms independently through a pseudopotential presented by Coker *et al.*[2] The electron–atom pseudopotential contains a polarization term $-e^2\alpha_0/2r^4$, which is the interaction between the electronic charge and the induced dipole moment on the xenon atom. It is necessary to go beyond this pair polarization model and to include many-body polarization effects because the polarizability α_0 of xenon is very large. Although many-body polarization effects on the solvation of classical cations in Xe clusters have been treated before,[3] this paper adresses the solvation of a quantum mechanical electron. Recently, Wallqvist *et al.*[4] showed that inclusion of many-body polarization contributions shifts the absorption spectrum of an excess electron in liquid water to the blue by approximately 0.2 eV and also gives rise to significant structural changes in the electron distributions.[6] Given the much larger polarizability of xenon than water, we expect much larger effects here.

It is easy to predict the qualitative effects of many-body polarization on the stability of Xe_n^-. The polarization energy will increase (become less negative) in going from the pair polarizability to the full many-body polarization calculation because the local electric field is smaller than the unscreened Coulomb field due to the electron. That is, the pair polarization model ignores the induced dipole–induced dipole interactions (i.e., considers only the unscreened Coulomb field) which are repulsive for near neighbor xenon atoms. Therefore, many-body polarization is expected to lead to a much weaker binding energy of the electron to the cluster. This destabilization of the cluster anions will cause the electron to become more extended than was found in our previous publication.[1]

In this paper the diffusion Monte Carlo method is used to compute the binding energy and structure of an excess electron to Xe_n as a function of cluster size n using a many-body polarization pseudopotential. The xenon atoms ($n < 19$) were frozen in the minimum energy geometries described by Hoare and Pal.[6,7] Finite temperature calculations performed on the full electron xenon system for the pair polarization model have shown that for small clusters the electron does not effect the xenon distribution.[1] A frozen xenon model is therefore perfectly adequate to determine ground state properties of the electron. The results of the diffusion Monte Carlo simulations of an excess electron in the frozen xenon system for the many-body polarization model are herein compared to those for the two-body model.[1] In agreement with qualitative predictions the electron is destabilized by the addition of many-body polarization. The smallest cluster found to bind an electron is Xe_6 with the pair additive polarization but is Xe_7 with many-body polarization. The binding energy, corresponding to the many-body

 0021-9606/89/073744-12$02.10

polarization model is found to be reduced by a global factor 2.7 from the pair polarization model and the electron is found to exist in a more diffuse surface state. As the electron is even more weakly bound in the many-body polarization model, we expect it to be even less likely to perturb the xenon distribution than the pair polarization model which again for small clusters caused no discernable changes in the distribution.

Recently, a dielectric continuum model was developed to calculate the electron binding energy to xenon clusters.[8] It is based on a model used by Cohen *et al.* to study surface states in liquid helium.[9] First, the electron–cluster interaction potential is determined from the electrostatic potential of a system consisting of a dielectric sphere and a point charge. The resulting "continuum" pseudopotential is then substituted into the Schrödinger equation which is solved to obtain ground state energies and wave functions. We compare this simple model and our microscopic model, and find that it gives reasonable agreement when a proper choice is made for the dielectric constant. Why should a continuum model which ignores the details of the electron–xenon potential surface agree with a microscopic model? A cluster may be approximated by a continuum model if the cluster is small enough that the associated electronic ground state is very diffuse, extending to large radial distances from the cluster, and therefore has small amplitude in the interatomic spaces. In this case, inaccuracies inside the cluster may not have large effects on the wave function. We expect that for much larger clusters, where the ground state is a bulk state, the dielectric continuum model will not agree with the microscopic model. Although we have not studied larger clusters here, we have compared the results of a pair polarization continuum model (defined as a limit of the many polarization model) with our microscopic pair polarization model. Poor agreement is found for all cluster sizes indicating a break down of the theory. If parameters are chosen to yield adequate results for small clusters, the results for larger cluster sizes $n \geqslant 15$ become inadequate as expected. This inadequacy at large cluster size is observed more quickly for pair polarization than for many body polarization because the omission of many-body effects allows the electronic ground state to become less extended. Again, in such cases, the channels discussed here and in previous papers play a dominant role that is ignored by continuum theories.

In this paper we also introduce a new fast Fourier transform projector method for determining the states of an excess electron bound to clusters. Previous FFT methods[10–12,15] are not suited to such calculations. This new method should therefore prove very useful for the study of bound and excited states of cluster anions.

II. METHODOLOGY

A. Many-body polarization

The many-body polarization potential for a point charge interacting with a set of polarizable atomic centers is[13,14]

$$V_p^{(\text{many-body})}(\mathbf{r}_e,\mathbf{r}) = -\frac{1}{2}\sum_{i=1}^{n} \boldsymbol{\mu}_i \cdot \mathbf{E}_i^0, \tag{2.1}$$

where the sum is over the polarizable centers, μ_i is the induced dipole moment of the ith polarizable center, $\mathbf{E}_i^{(0)}$ is the electric field on the ith center due to the point charge which is given by,

$$\mathbf{E}_i^{(0)} = e\mathbf{r}_{ie}/r_{ie}^3, \tag{2.2}$$

where r_{ie} is the distance from the point charge to the ith polarizable center. The induced dipole moment of the ith center is defined as

$$\boldsymbol{\mu}_i = \alpha_0 \mathbf{E}_i, \tag{2.3}$$

where $\mathbf{E}_i$ is the local electric field acting on the ith center, and α_0 is the static polarizability of atomic Xe;

$$\mathbf{E}_i = \mathbf{E}_i^{(0)} - \alpha_0 \sum_{k\neq i=1}^{n} \mathbf{T}_{i,k}\cdot\mathbf{E}_k \tag{2.4}$$

and $\mathbf{T}_{i,k}$ is the second rank tensor representing the dipole propagator,

$$\mathbf{T}_{i,k} = \left[\mathbf{I} - \frac{3\mathbf{r}_{ik}\mathbf{r}_{ik}}{r_{ik}^2}\right]\frac{1}{r_{ik}^3}. \tag{2.5}$$

It should be noted that if many-body effects are ignored one calculates the induced dipole using only the bare Coulomb electric field,

$$\boldsymbol{\mu}_i = \alpha_0 \mathbf{E}_i^{(0)}. \tag{2.6}$$

In classical electrostatics one solves Eq. (2.4) for the electric fields at the atomic centers and computes the induced dipoles. Then, the induced dipoles and the electric fields can be used to compute the polarization energy $V_p^{\text{many-body}}$. This is not appropriate quantum mechanically because the polarization interaction will be reduced as the electron penetrates the core electrons of an atom.[13] In fact, in the electron–xenon pseudopotential the two-body polarization potential[3] is multiplied by a switching function $S(r)$ such that;

$$V_p^{(\text{pair})}(\mathbf{r}) = -e^2\alpha_0 S(r)/2r^4 \tag{2.7}$$

with

$$S(r) = 1 - [1 + (fr) + 2(fr)^2 + 4/3(fr)^3 + 2/3(fr)^4 + 4/27(fr)^5]\exp[-2fr], \tag{2.8}$$

where $S(r)$ turns off the effective charge as $r\to 0$, $f = 0.638\,411\,7\alpha_0^{-1}$, and $\alpha = 27.09\,a_0^3$. Thus, to treat many-body polarization in xenon, we simply allow the charge seen by each xenon atom to be a function of the electron–atom distance. This, of course, modifies the corresponding Coulomb field in Eq. (2.4).

$$\mathbf{E}_i^{(0)} = eS(r_{ie})^{1/2}\mathbf{r}_{ie}/r_{ie}^3. \tag{2.9}$$

With this modification of the Coulomb field the many-body polarization energy is computed in the same manner as is described above for classical electrostatics. It is easy to see that the resulting formulation for the polarization energy reduces to Eq. (2.7) for the case of one xenon atom and one electron. Finally, the full potential energy can be expressed using our fit to the full pseudopotential,[3] the two-body polarization energy and the many-body polarization energy.

$$V(\mathbf{r}_e,\mathbf{r}) = \sum_{i=1}^{n}[V_{\text{tot}}^{(\text{fit})}(\mathbf{r}_{ie}) - V_p^{(\text{pair})}(\mathbf{r}_{ie})] + V_p^{(\text{many-body})}(\mathbf{r}_e,\mathbf{r}). \tag{2.10}$$

Here $V_{\rm tot}^{\rm (fit)}$ in atomic units is

$$V_{\rm tot}^{\rm (fit)}(r) = \left[\frac{4920}{(3793 + r^6)} - 1\right]\frac{12.59}{r^4}. \quad (2.11)$$

Two methods were used to simulate the Xe_n^- anions on this potential energy surface: diffusion Monte Carlo and the projector method.

B. Diffusion Monte Carlo

Difffusion Monte Carlo[15–17] is based on solving the imaginary time Schrödinger equation. For an electron moving in a potential field of n frozen xenon atoms this equation is

$$\frac{\partial\psi(\mathbf{r},\tau)}{\partial\tau} = -\hat{H}\psi(\mathbf{r},\tau) = \left[\frac{\hbar^2}{2m_e}\nabla^2 - [V(\mathbf{r}) - V_{\rm ref}]\right]\psi(\mathbf{r},\tau), \quad (2.12)$$

where $V_{\rm ref}$ is a reference energy and $V(\mathbf{r})$ is described above. This equation can be transformed from an equation for $\psi(\mathbf{r},\tau)$, the wave function, to an equation for $f(\mathbf{r},\tau) = \psi(\mathbf{r},\tau)\psi_T(\mathbf{r})$, where ψ_T is an arbitrary function of the electron coordinates.[18,19]

$$\frac{\partial f(\mathbf{r},\tau)}{\partial\tau} = \frac{\hbar_2}{2m_e}\nabla^2 f(\mathbf{r},\tau) - \frac{\hbar^2}{m_e}\nabla[f(\mathbf{r},\tau)\cdot\nabla\log\psi_T(\mathbf{r})] - \left[\frac{H\psi_T(\mathbf{r})}{\psi_T(\mathbf{r})} - V_{\rm ref}\right]f(\mathbf{r},\tau). \quad (2.13)$$

This equation is simulated by dividing τ into small intervals $\Delta\tau$ such that each term in the equation can be considered independent. An ensemble of electrons representing $f(\mathbf{r},\tau)$ is then propagated according to the independent pieces of Eq. (2.12). Such a procedure that allows large values of $\Delta\tau$ to be used is outlined by Anderson.[20] At large values of $\tau = n\Delta\tau$ the ensemble will have decayed to $\psi_0\psi_T$, where ψ_0 is the ground state wave function.

As in the previous paper[1] a pair product form was taken for ψ_T.

$$\psi_T(\mathbf{r}) = \prod_{i=1}^{n} h(|\mathbf{r} - \mathbf{R}_i|) \quad (2.14)$$

Again, two different functional forms for $h(r)$ were used in the present calculation. The first is the zero energy s-wave solution to the Schrödinger equation for the interaction of an electron with a single xenon atom.[21]

$$\left[\frac{\hbar^2}{2m_e}\nabla^2 - V_{e\text{-Xe}}(r)\right]rh_1(r) = 0, \quad (2.15)$$

$h_1(r)$ was chosen because it has no variational parameters. Simulations based on Eq. (2.13) using $h_1(r)$ as the importance sampling function, were performed to determine the set of clusters that would bind the electron. Having determined which electron–cluster systems were bound, variational calculations were performed on these systems using a second function

$$h_2(r) = \frac{1}{r^{1/n}}\exp\left[-\frac{\gamma'}{r(r^3 + c)} - \alpha r\right]. \quad (2.16)$$

The additional term $r^{1/n}$ added to h_2 of the previous paper[1] was found to improve the variational energies considerably. All constants are variationally adjusted. The variational integrals were evaluated numerically using a three dimensional quadrature.[22] The resulting ψ_T was sufficiently close to the ground state wave function that potential and kinetic energy and structure could be calculated using the interpolation formula.[19]

$$\langle A\rangle_{\psi^2} \cong 2\langle A\rangle_f - \langle A\rangle_{\psi_T^2}. \quad (2.17)$$

The total energy E_0 can be calculated by averaging $\hat{H}\psi_T/\psi_T$.

$$\left\langle\frac{\hat{H}\psi_T}{\psi_T}\right\rangle_f = \frac{\int\psi_0\psi_T(\hat{H}\psi_T)/\psi_T dv}{\int f dv} = \frac{\int\psi_T\hat{H}\psi_0 dv}{\int f dv} = E_0. \quad (2.18)$$

The coarse simulations using h_1 were run for 15 000 times steps of length 0.6 a.u. Averages were kept over the last 10 000 steps. The simulations using importance sampling function h_2 were run for 50 000 time steps of length 0.4 a.u. Averages were kept over the last 40 000 steps of a run.

C. Projector method

Another method for determining the allowed energies and energy eigenfunctions of a given Hamiltonian is to recognize that if ψ is a function that is strictly orthogonal to all of the first n energy eigenstates $\psi_0,\ldots\psi_{n-1}$ the

$$\lim_{\beta\to\infty}\exp[-\beta\hat{H}]\psi = \exp[-\beta E_n]\psi_n \quad (2.19)$$

(Note that this relationship is used in diffusion Monte Carlo with $n = 0$).

In order to utilize Eq. (2.19) a way must be found to apply the propagator to a given wave function. One method is to expand the wave function in a complete set of states which are eigenfunctions of Hamiltonian $\hat{H}_0$ and use a "short time" split operator approximation to evaluate the propagator.

$$\exp\left[-\frac{\beta}{P}(\hat{H} - \hat{H}_0 + \hat{H}_0)\right]^P = \prod_{i=1}^{P}\exp\left[-\frac{\beta}{2P}(\hat{H} - \hat{H}_0)\right]\times\exp\left[-\frac{\beta}{P}\hat{H}_0\right]\exp\left[-\frac{\beta}{2P}(\hat{H} - \hat{H}_0)\right]. \quad (2.20)$$

If $\hat{H}_0$ is chosen such that $(\hat{H} - \hat{H}_0)$ contains no differential operators, it is easy to evaluate Eq. (2.19). One simply transforms between two Hilbert spaces, position space and the space of the eigenfunctions of $\hat{H}_0$ and at each step modifies the resulting distribution at each point in the given space by $\exp[-\beta(\hat{H} - \hat{H}_0)/2P]$ and $\exp[-\beta E_n/P]$, respectively. However, because we cannot, in general, perform the transformations analytically on the full Hilbert space we must truncate both spaces. That is we use a finite number of eigenfunctions and a finite number of points in position space. However, in order for Eq. (2.19) to converge, the eigenfunctions must be strictly orthogonal in the finite Hilbert space.

The usual choice to take for $\hat{H}_0$ is the kinetic energy

operator. $\hat{T}$.[10–15] The wave function can be expanded as[10–15]

$$\psi = \sum_{k=1}^{N} \exp[2\pi ikx/L\,], \tag{2.21}$$

where L is some cutoff in position space. The finite position space is defined to be

$$x_j = (j-1)L/N j = 1,N. \tag{2.22}$$

It is easy to show that the basis wave functions are orthogonal on this finite space. We are not, however, limited by this choice. The most useful extension of this is to choose $\hat{H}_0$ such that its eigenfunction are orthogonal polynomials. Gaussian-type quadrature points (degree $n+1$) can then be used to define the finite position space. The harmonic oscillator, the morse oscillator (bound states), and the rigid rotor Hamiltonian (specifically the associated legendre polynomials) all come to mind. The advantage of using Fourier representation is that the number of operations for a transform is only $N\log(N)$, however, the gain in efficiency by using a more appropriate basis may be considerable.

The Fourier basis is a poor choice for electron–cluster systems where the electron is found in an extended or diffuse surface state. The points of the finite position space are spread equally throughout the interval. Since the electron wave function only changes rapidly near the cluster and the wave function extends far from the cluster this is very inefficient. A better choice is to expand the wave function as

$$r\psi = \sum_{m=-N}^{N} \sum_{l=|m|}^{N} \sum_{k=1}^{N'} \sin(\pi kr/L) S_l^m(x) \exp[im\phi], \tag{2.23}$$

where $x = \cos(\theta)$ and the $S_l^m(x)$ are the associated Legendre functions. If we now propagate $r\psi$, instead of ψ, the propagator is

$$\exp[-\beta\hat{H}\,] = \exp\left\{-\beta\left[-\frac{\hbar^2}{2m}\frac{\partial^2}{\partial^2 r} + \hat{L}/(r^2+\hat{V})\right]\right\}. \tag{2.24}$$

The position space is defined by equally spaced points in r and ϕ and standard Gaussian quadrature points in x. It can be shown that a sine transform is orthogonal over this basis and that the $S_l^m(x)$ are orthogonal over the Gaussian quadrature basis for the same m. Also, these quadrature points are spaced to efficiently reproduce the variation of the wave function close to the origin. The short time approximation used is

$$\exp[-\beta\hat{H}\,] = \exp\left[-\frac{\beta\hat{V}}{2}\right]\exp\left[-\frac{\beta\hat{L}}{2\hat{r}^2}\right] \tag{2.25}$$

$$\times\exp\left[\frac{\beta\hbar^2}{2m}\frac{\partial^2}{\partial^2 r}\right] \tag{2.26}$$

$$\times\exp\left[-\frac{\beta\hat{L}}{2\hat{r}^2}\right]\exp\left[-\frac{\beta\hat{V}}{2}\right]$$

Thus, a half-propagation consists of a multiplication of the wave function in position space, a Fourier transform from ϕ to m, an associated Legendre transform from x to l followed by a multiplication in l, m, r space, a sine transform, and a multiplication in l, m, k space. Note that only the associated Legendre transform cannot be calculated with a FFT (A sine transforms may be expressed as a FFT with twice as many points).

The method was applied to Xe_{13}^- for both the pair polarization model and the many-body polarization model. For both models a time step of $\tau = 0.03$ was used with a grid size of 256 points in r and 32 points in both x and ϕ. For the pair polarization model r was allowed to range from 0 to 18σ while for the many-body polarization model r was allowed to range from 0 to 30σ. In both cases the grid was centered on the center of mass of the cluster. It was therefore easy to calculate radial distributions centered on the center of mass.

III. RESULTS

A. Diffusion Monte Carlo simulations of Xe_n^-

The ground state energy of an excess electron in each of a series of xenon clusters was determined by diffusion Monte Carlo simulations using the importance sampling function h_1 defined in Eq. (2.15). Many-body polarization was included explicitly using Eqs. (2.1) and (2.4). Variational calculations were then performed using the function h_2 defined in Eq. (2.16) (see Table I). Diffusion Monte Carlo simulations using this optimized function h_2 gave refined ground state energies and allowed determination of the potential energy, kinetic energy and the structure of the electron in each of the clusters. All calculations were performed with the xenon atoms frozen in their neutral lowest energy geometry. In our first paper we have shown in finite temperature simulations on the entire electron xenon system using the pair polarization model that the electron induces no changes in the xenon distribution for small clusters. We expect the same will true for the many-body polarization model as the electron will be shown to be less strongly bound than in the pair polarization model and thus less able to induce changes in the xenon distribution.

The ground state energy of an excess electron in xenon cluster anions, Xe_n^-, with n ranging from 6 to 19 are plotted in Fig. 1(a) where they are compared to the results obtained using the pair polarization model. The effect of many-body polarization, is quite remarkable. Xe_6, found to bind an excess electron with pair polarization, does not with many-

TABLE I. Variational calculations: Many-body polarization.

Cluster	E_{exact}/K	$\langle E\rangle/K$	α(a.u.)
Xe_7^-	-6 ± 1	1	0.0013
Xe_8^-	-24 ± 2	-16	0.0015
Xe_9^-	-50 ± 2	-42	0.002
Xe_{10}^-	-85 ± 2	-73	0.0025
Xe_{11}^-	-122 ± 2	-108	0.0025
Xe_{12}^-	-157 ± 2	-137	0.0027
Xe_{13}^-	-161 ± 2	-145	0.0024
Xe_{14}^-	-197 ± 3	-175	0.0024
Xe_{15}^-	-232 ± 3	-205	0.0024
Xe_{16}^-	-269 ± 3	-238	0.0024
Xe_{17}^-	-304 ± 4	-275	0.00255
Xe_{18}^-	-335 ± 4	-303	0.00255
$\gamma = 161$	$c = 70$		

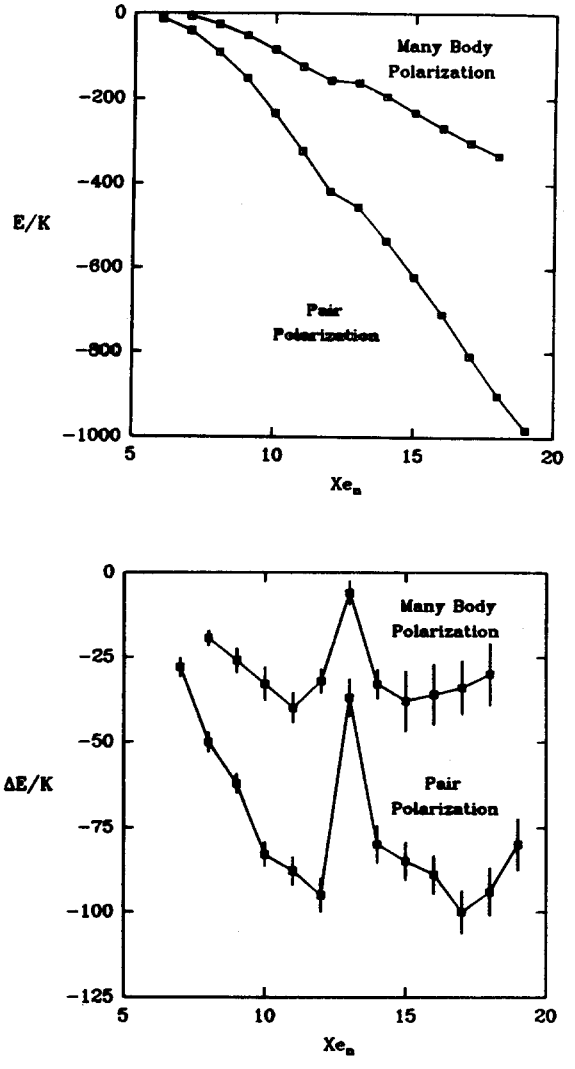

FIG. 1. The ground state energy of an excess electron in Xe_n as a function of cluster size n. Energies calculated using the pair polarization model are compared to those calculated using the many-body polarization model. The second figure shows the difference between the ground state energy of an excess electron in Xe_n and Xe_{n+1} as a function of cluster size, again for both the pair and many-body polarization methods.

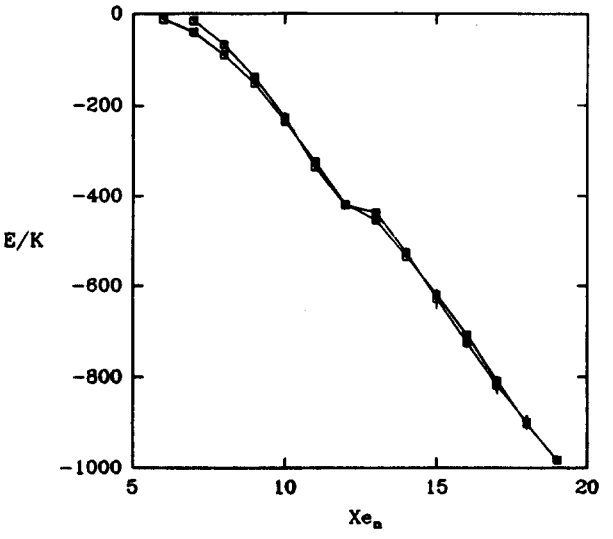

FIG. 2. The ground state energy of an excess electron in Xe_n as a function of cluster size n. Energies calculated using the pair polarization model are compared to those calculated using the many-body polarization model multiplied by a constant ($c = 2.7$).

body polarization. In fact, the ground state energy decreases by a factor of approximately 2.7 for all clusters, but the detailed features of the curve remain the same on that scale (see Fig. 2). That is, for both the pair and many-body polarization models, the ground state energy decreases monotonically with a reduction in slope between Xe_{12}^- and Xe_{13}^- [see Fig. 1(b)] due to the contraction of the cluster when it completes a shell to become an icosohedron as discussed in the previous paper.[1] Note that the energies for pair polarization are slightly different for the larger clusters than those presented in the previous paper. The improved form of h_2 (see Table II for variational parameters for two-body polarization) and a faster computer allowed the use of a smaller time step 0.05 a.u. which was needed to insure convergence of the energies of the larger clusters. (The percent error induced by the larger time step decreased from 6% at Xe_{19}^- to ~0% at Xe_9^-.)

Figure 1(b) shows the, $\Delta E_0 = E_0(n+1) - E_0(n)$, increment (rate of change) in the ground state energy on adding one more xenon atom to the cluster as a function of cluster size n. After an initial rapid decrease, the rate of change begins to level off and become relatively constant except at $n = 12,13$ as previously discussed. Linear least squares fits of the energy as a function of cluster size n,

$$E_0(n) = a \cdot n + b \tag{3.1}$$

are summarized in Tables III and IV for many-body and pair polarization, respectively. Briefly, the slopes are approximately -35 K/atom for many-body polarization and -89 K/atom for pair polarization. Of course, for very large clusters where the electron becomes fully solvated; that is, forms a bulk state, the addition of one xenon atom to the cluster should not change the electron binding energy. However, for the small clusters studied here, the electronic ground state

TABLE II. Variational calculations: Pair polarization.

Cluster	E_{exact}/K	$\langle E\rangle/K$	α(a.u.)
Xe_6^-	-12 ± 2	-6	0.0008
Xe_7^-	-40 ± 2	-34	0.0017
Xe_8^-	-90 ± 2	-83	0.0025
Xe_9^-	-152 ± 2	-145	0.003
Xe_{10}^-	-235 ± 3	-226	0.0035
Xe_{11}^-	-323 ± 3	-312	0.0039
Xe_{12}^-	-418 ± 4	-401	0.0042
Xe_{13}^-	-455 ± 4	-439	0.004
Xe_{14}^-	-535 ± 4	-515	0.004
Xe_{15}^-	-620 ± 4	-599	0.0041
Xe_{16}^-	-709 ± 4	-687	0.0042
Xe_{17}^-	-809 ± 5	-780	0.0043
Xe_{18}^-	-903 ± 5	-871	0.0043
Xe_{19}^-	-983 ± 6	-948	0.0044
$\gamma = 92$	$c = 40$		

TABLE III. Linear least squares fits to the ground state energetics (many-body polarization) $y(n) = a \cdot n + b$ and r is the correlation coefficient.

Quantity	Xe_n^-	a	b	$\|r\|$
	$n = 9$–12	−35.5	269.0	0.999
E_0/K	$n = 13$–18	−34.7	288.9	0.999
	$n = 9$–18	−30.7	223.0	0.996
	$n = 7$–18	−144	619.1	0.987
$\langle V \rangle/K$	$n = 7$–12	−203	1160	0.995
	$n = 13$–18	−136	527.9	0.997
	$n = 7$–18	115	−409.4	0.979
$\langle T \rangle/K$	$n = 7$–12	175	−961.9	0.995
	$n = 13$–18	103	−257.1	0.994

has a large, diffuse, surface component as shown later, and the binding energy changes linearly with cluster size.

The monotonic increase of binding energy with cluster size and the dramatic decrease in binding energy with the addition of many-body polarization can be explained by microscopic considerations. Deep channels of electronic potential energy run through a xenon cluster. The channels are formed because the minimum of the electron xenon pseudopotential occurs at $r_{e\text{-}Xe} = d_{min}/2$ where d_{min} is the minimum of the xenon–xenon potential. Thus, for xenon atoms placed at the lowest neutral cluster energy configuration (though as previous stated the electron should not modify

TABLE IV. Linear least squares fits to the ground state energetics (pair polarization) $y(n) = a \cdot n + b$ and r is the correlation coefficient.

Quantity	Xe_n^-	a	b	$\|r\|$
	$n = 9$–12	−88.6	648.3	0.999
E_0/K	$n = 13$–19	−89.6	717.4	0.999
	$n = 9$–19	−82.1	591.2	0.998
$\langle V \rangle/K$	$n = 7$–19	−332	1601	0.996
$\langle T \rangle/K$	$n = 7$–19	252	−1049	0.994

these positions), the minima of the electron xenon pseudopotential overlap forming a chnnel. The channels of Xe_3^- are displayed in Fig. 3. The binding energy of the electron will increase with the number and depth of the channels. The addition of a xenon atom to a cluster, provides just this effect. Therefore, the binding energy of the excess electron increases with cluster size. Many-body polarization lowers the binding energy by changing the depth of the channels. Essentially, the many-body polarization ansatz allows the dipoles induced on the xenon atoms by the presence of the electron to interact through the dipole tensor. Pair polarization does not include these induced dipole–induced dipole interactions. These interactions add repulsive energy to the system and substantially decrease the depth of the channels. This can be seen in Fig. 4 where the absolute minima of the

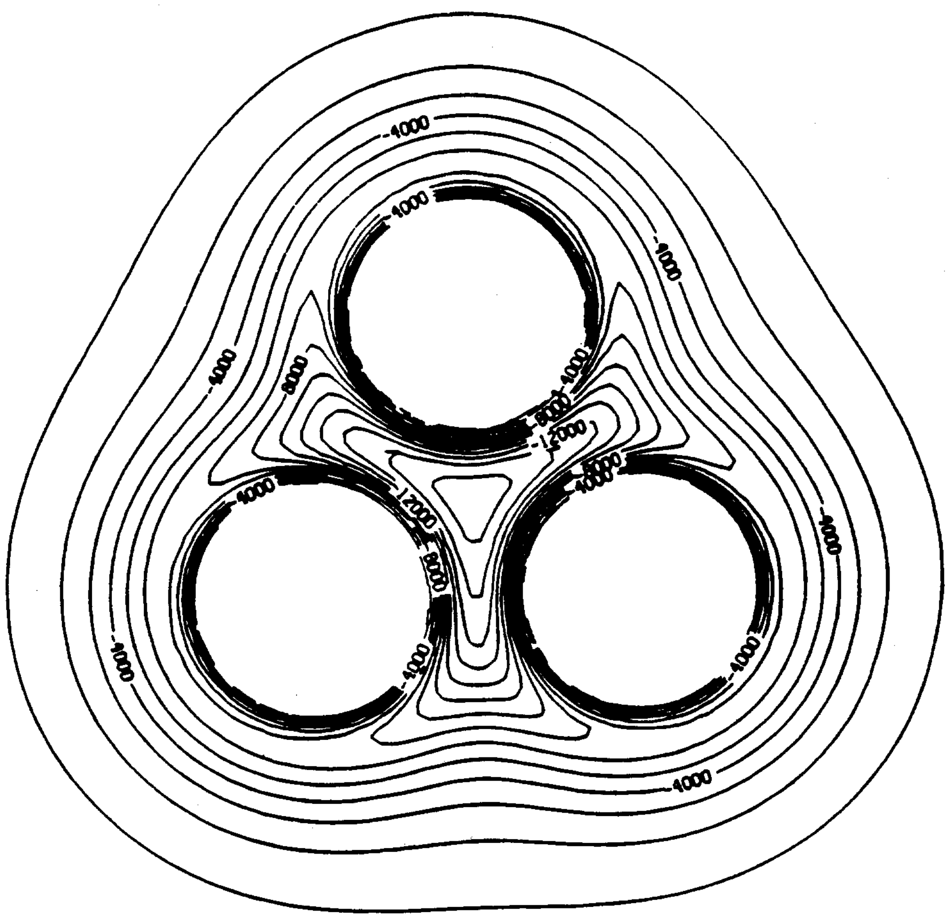

FIG. 3. The potential energy surface ($z = 0$) of Xe_3^- for the polarization model.

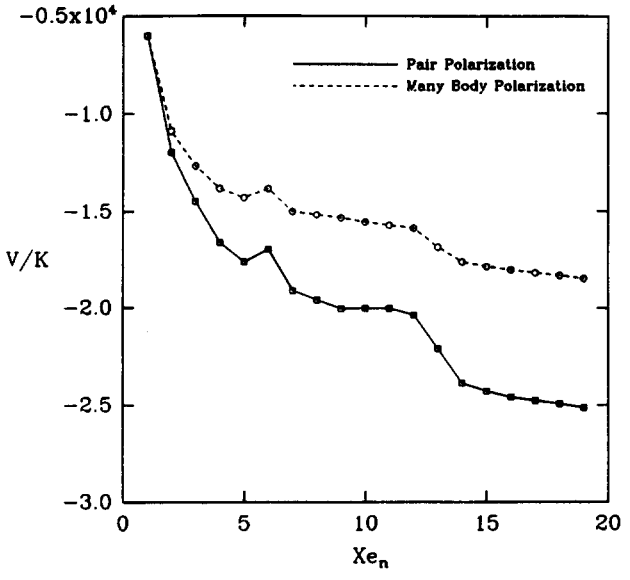

FIG. 4. The absolute minimum of electronic potential energy as a function of cluster size n. Minima calculated using the pair polarization model are compared to those calculated using the many-body polarization model.

electron–xenon potential energy surface for many-body polarization and two-body polarization are plotted vs cluster size. It must be stated that despite the change in depth of the channels, their general shape remains unchanged. The shape of the channels is determined by the xenon–xenon potential energy (which determines the xenon position) and the "hard core" of the pseudopotential which is not effected by many-body polarization. Thus, the depth of the potential energy surface is changed only around the minima. The many-body polarization potential is, again, less attractive than the two-body polarization potential in the channels. We therefore expect that the electron will be more extended, and from the virial theorem we expect it to have a smaller kinetic energy in the system with many-body polarization. The decrease in kinetic energy does not spring from the short range repulsive interactions (which are unchanged) but from the trivial delocalization effect caused by the reduction in the channel attractions.

The spatial distribution of the electron on the xenon clusters was also markedly changed by the inclusion of many-body polarization. The electron is much more extended with many-body polarization than is the case when only pair polarization is considered. As in our previous work, we define $P(r)$ to be the probability distribution function of the electron position with respect to the center of mass of the xenon cluster, and $g(r)$ is defined as the electron density at a distance r from a xenon atom averaged over all xenon atoms $[\int 4\pi r^2 g(r) = n]$. In Fig. 5, $P(r)$, is shown for a number of clusters both with and without many-body polarization. The effect of many-body polarization is again to delocalize the electron. For example, $P(r)$ for Xe_{13}^- with pair polarization the electron probability peaks at 0.42 while with many-body polarization, the probability peaks at 0.29 and extends much further from the cluster. The $g(r)$ shown in Fig. 6 also exhibits the decreased localization. Again the peak heights are noticeably smaller when many-body polarization is included, due to the increase in the potential energy in the channels. Note, the effect of the channels may be seen in the $g(r)$ as the first peak occurs at $d_{\min}/2$ and the second peak occurs at $3d_{\min}/2$.

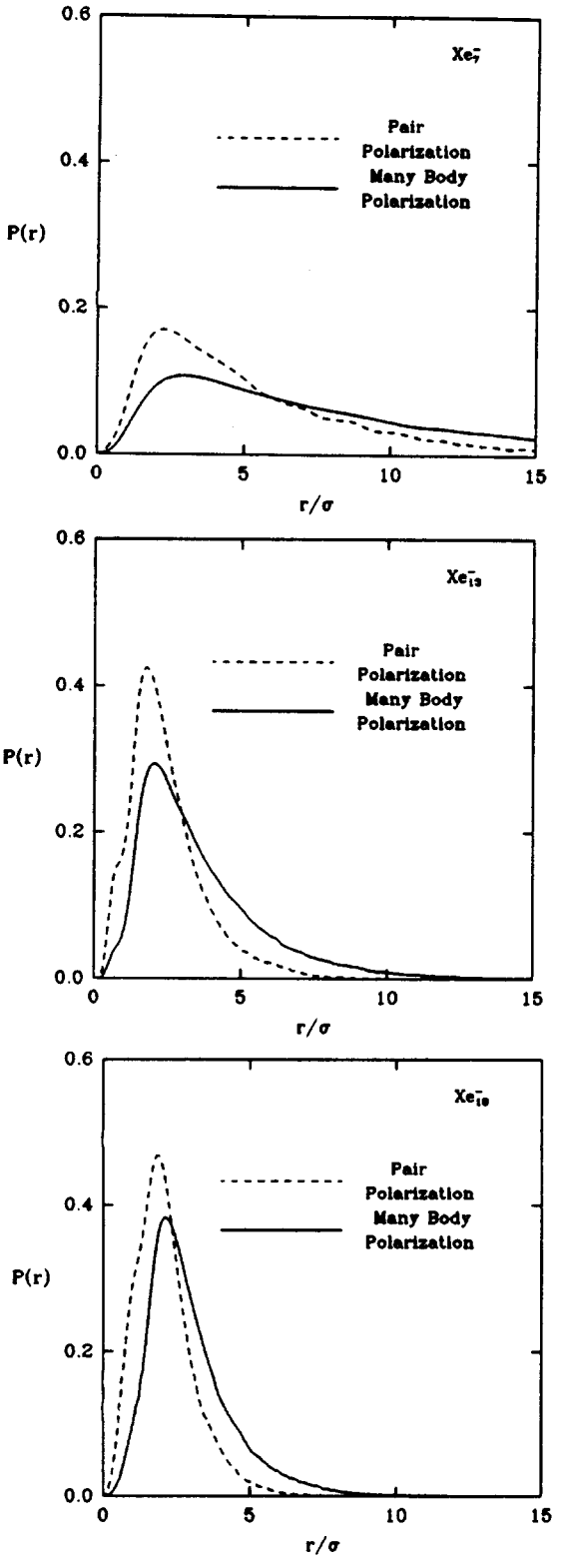

FIG. 5. The electron probability distribution function of electron position with respect to the cluster center of mass $P(r)$ for three cluster sizes. Distributions calculated using many-body polarization are compared to those calculated using pair polarization.

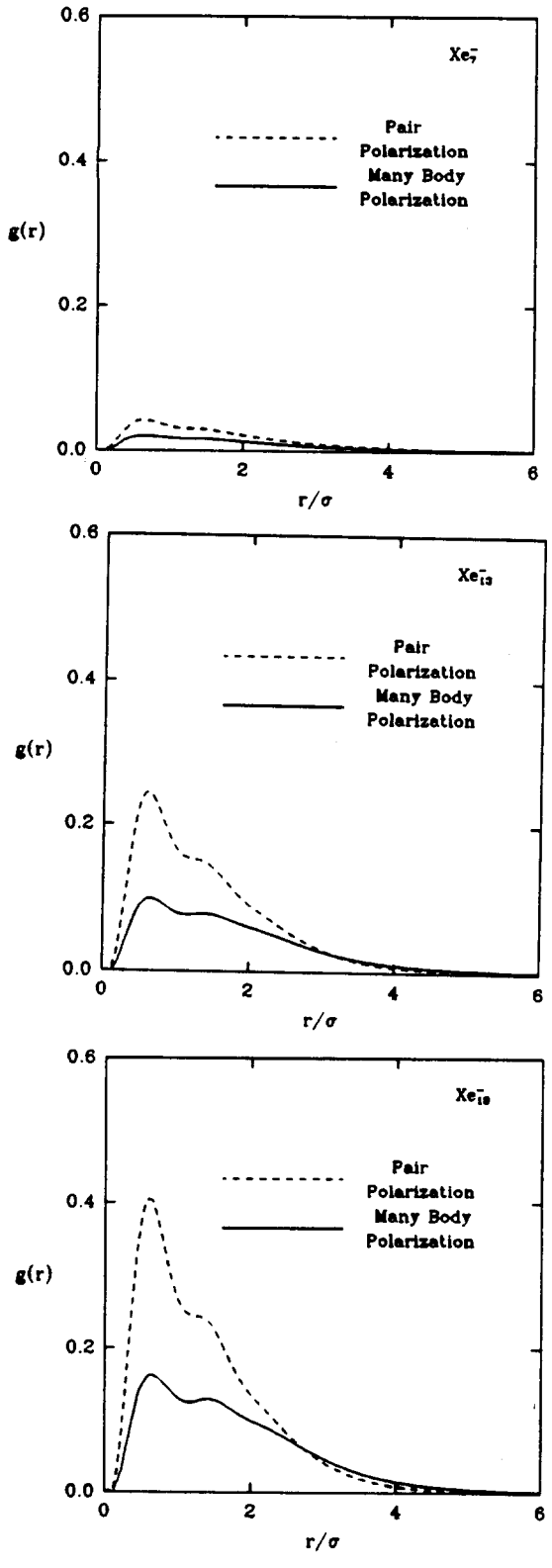

FIG. 6. The electron–xenon pair distribution functions $g(r)$ for three cluster sizes. Distributions calculated using many-body polarization are compared to those calculated using pair polarization.

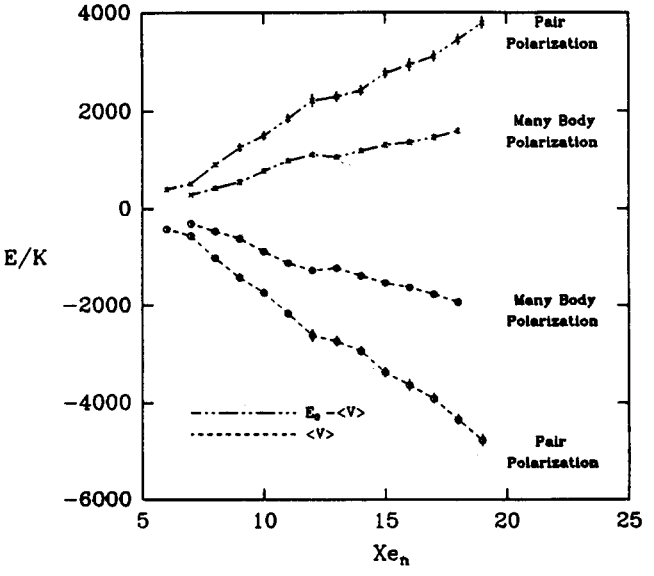

FIG. 7. The potential and kinetic energy of an excess electron as a function of cluster size n. The potential and kinetic energy calculated using many-body polarization are compared to those calculated using pair polarization.

The effect of many-body polarization on the potential and kinetic energy of the electron in xenon clusters is commensurate with the effect on the structure. Both the kinetic and potential energy are reduced from their values when only pair polarization is considered. This can be observed in Fig. 7. The kinetic energy is reduced from its value with pair polarization because the electron is less localized than with pair polarization. The potential energy is reduced both because the electron is less localized in the potential channels within the cluster and because the channels are not as deep. A linear least square fit of the potential and kinetic energies vs cluster size is given in Tables III and IV.

B. Projector method

The projector method outlined in Sec. II was applied to Xe_{13}^- for both the pair polarization and many-body polarization models. The energies obtained by diffusion Monte Carlo and by the projector method for the two models agree well as do estimates of the potential and kinetic energies (see Table V). Note also that the virial theorem

$$\langle T\rangle + \langle V\rangle = E,$$
$$2\langle T\rangle = \langle \mathbf{r}\cdot\nabla V\rangle \qquad (3.2)$$

applied to the wave functions obtained by the projector method holds (± 2 K), an indication of the quality of the wave functions. A comparison of the electron xenon com $P(r)$ produced by the two different methods are shown in Figs. 8 and 9. Figure 8 presents the comparison for the pair polarization and Fig. 9 for many-body polarization. Again the agreement is very good. The differences can be accounted for by time step error and noise on the diffusion Monte Carlo data. The advantage of the FFT method is that it gives the total wave function and there are no statistical fluctuation inherent in the method. However, only for the mnay-body polarization does it become computationally competitive. The additional advantage of this method is that excited states can be examined with no additional complications. However, bound excited states are only likely to exist in larger clusters than those studied here. The need for a variational wave function is not eliminated as the algorithm is much

TABLE V. Comparison of diffusion Monte Carlo (DMC) and the projector method (PM) for both the pair and many-body polarization models.

Quantity	Pair(DMC)	Pair(PM)	Many-body(DMC)	Many-body(PM)
E_0/K	-453 ± 4	-453	-159 ± 3	-157
$\langle V \rangle/K$	-2687 ± 100	-2711	-1209 ± 50	-1180
$\langle T \rangle/K$	...	2257	...	1025

more efficient if a reasonable approximation to ψ_0 is used to begin the propagation.

IV. DISCUSSION

Many-body polarization has been shown to be extremely important consideration in electron attachment to xenon clusters. Though the xenon atoms were held fixed in their energy lowest neutral configuration this was shown in our previous paper[1] to be quite reasonable and the results described herein can be considered valid. Many-body polarization increases the minimum number of xenon atoms needed to bind an electron from six to seven and drastically changes the binding energy of the electron to larger clusters. The excess electron charge distribution as well as its kinetic and potential energy are also dramatically changed. Xenon does perhaps represent an extreme limit in polarization effects both because it is very polarizable and has no permenent dipole moment. (The polarization interaction is the sole mechanism for binding the electron.) It also suggests that many-body polarization effects are in general of importance in electron attachment and solvation problems.

We have reported here that the ratio of the binding energy calculated in the pair polarization approximation to the binding energy including total many-body polarization is approximately a constant (equal to 2.7) as a function of cluster size. The kinetic energy and the potential energy also separately scale such that the potential energy corresponding to many-body polarization is a factor of 2.14 smaller than for pair polarization and the kinetic energy corresponding to many-body polarization is a factor of approximately 2.04 smaller than for pair polarization (although the scaling of the potential and kinetic energies is less precise than the scaling of the total energy). Again, linear least square fits of the potential and kinetic energies versus cluster size are given in Tables III and IV. Why should these simple scaling relationships exist? This is a difficult problem to tackle analytically and is not yet resolved. However, it will be shown that a dielectric agrument with no adjustable parameters does not predict the correct scaling.

It is interesting to determine how well a dielectric continuum model of a xenon cluster can estimate the structure and binding energy of an excess electron. This problem was considered by Stampfli *et al.*[2] Their approach was to determine the electrostatic potential for a dielectric sphere of radius R for two cases: the electron outside the sphere ($r_e > R$) and the electron outside the sphere ($r_e < R$). The potential energy felt by the electron, determined from the electrostatic potential, is then found to be

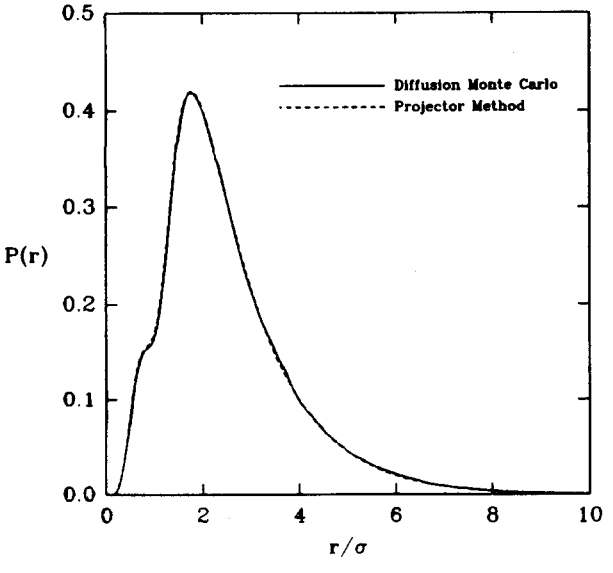

FIG. 8. The electron probability distribution function of electron position with respect to the cluster center of mass $P(r)$ for Xe_{13}^- modeled with pair polarization. The results of the projector method are compared to those of diffusion Monte Carlo.

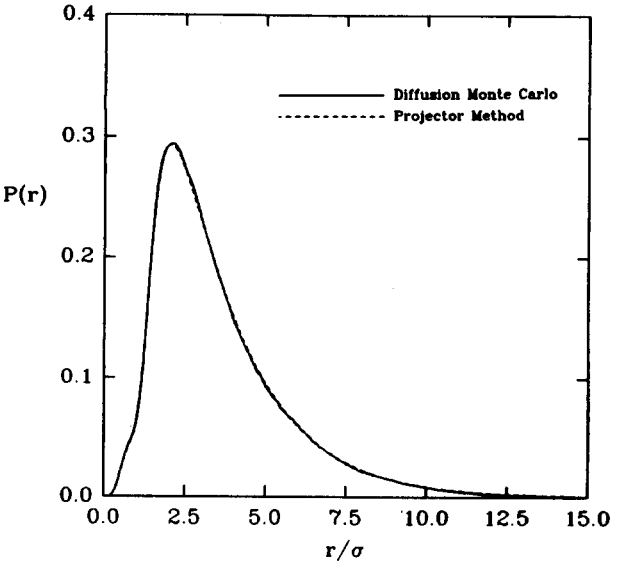

FIG. 9. The electron probability distribution function of electron position with respect to the cluster center of mass $P(r)$ for Xe_{13}^- modeled with many-body polarization. The results of the projector method are compared to those of diffusion Monte Carlo.

$$V_>(r_e) = -\frac{e^2(\epsilon-1)}{2}\sum_{k=1}^{\infty}\frac{k}{k\epsilon+k+1}\frac{R^{2k+1}}{r_e^{2k+2}}\, r_e > R, \tag{4.1}$$

$$V_<(r_e) = \frac{e^2(\epsilon-1)}{2\epsilon}\sum_{k=0}^{\infty}\frac{k+1}{k\epsilon+k+1}\frac{r_e^{2k+1}}{R^{2k+2}}\, r_e < R, \tag{4.2}$$

where ϵ was taken to be unity outside the media. Since the potential energy diverges at $r_e = R$ Stampfli *et al.*[2] propose the following modification:

$$\begin{aligned} &V(r_e) = V_>(r_e), \quad r_e > R+d, \\ &V(r_e) = V_<(R+d), \quad R-d < r_e < R+d, \\ &V(r_e) = V_<(r_e) - V_<(R-d) + V_>(R+d), \\ &r_e < R-d. \end{aligned} \tag{4.3}$$

This is reasonable because dielectric models break down for distances on the order of the molecular size and the divergence is simply a consequence of this fact. d is therefore chosen to reflect the molecular size.

$$d = \left(\frac{3}{4\pi\rho}\right)^{1/3}. \tag{4.4}$$

In order to account for the repulsive interactions V_R and interactions with neighboring atoms V_N which occur inside a real cluster a small constant is added to the potential defined in Eq. (4.13) for $r < R$. A reasonable estimate of these effects is

$$V_R + V_N = V_0 + \frac{e^2}{4d}(1-\epsilon^{-1}), \tag{4.5}$$

where V_0 is ground state energy of an electron in fluid xenon and $-e^2/4d(1-\epsilon^{-1})$ is a dielectric continuum estimate of the potential energy of the fluid.[2] The dielectric constant is then chosen to be given by the Clausius Mossotti relation which is correct for a structureless fluid

$$\epsilon = \frac{(1+8\pi\rho\alpha/3)}{(1-4\pi\rho\alpha/3)}. \tag{4.6}$$

The resulting potential can be inserted into a radial Schrödinger equation which we solved by a shooting method due to Johnson.[23] The results of this model for both the energy and the strucutre $[P(r)]$ are in remarkable agreement with our results for the following parameters: ($\rho = 0.014$ A^3, $V_0 = -0.65$ eV, $\alpha = 4.05$ A^3). Figure 10 shows the comparison of both the ground state energy as a function of cluster size $n = \rho^{1/3}R$ and the ground state wave function of Xe_{13}^- for the two models. Why is the agreement so good? Simply, there is very little electron amplitude inside the cluster and therefore a continuum model might be expected to work. However, one can see that the continuum model misses the shoulder of the wave function which is a signature of the channels, a microscopic feature. Since these features will become more important in larger clusters where the electron distribution is more structured the continuum model will begin to fail. In order to further test the applicability of the continuum model, a pair polarization limit of the potential was taken:

$$V_{\text{two-body}} = V_{\text{many-body}} + 0(\alpha^2). \tag{4.7}$$

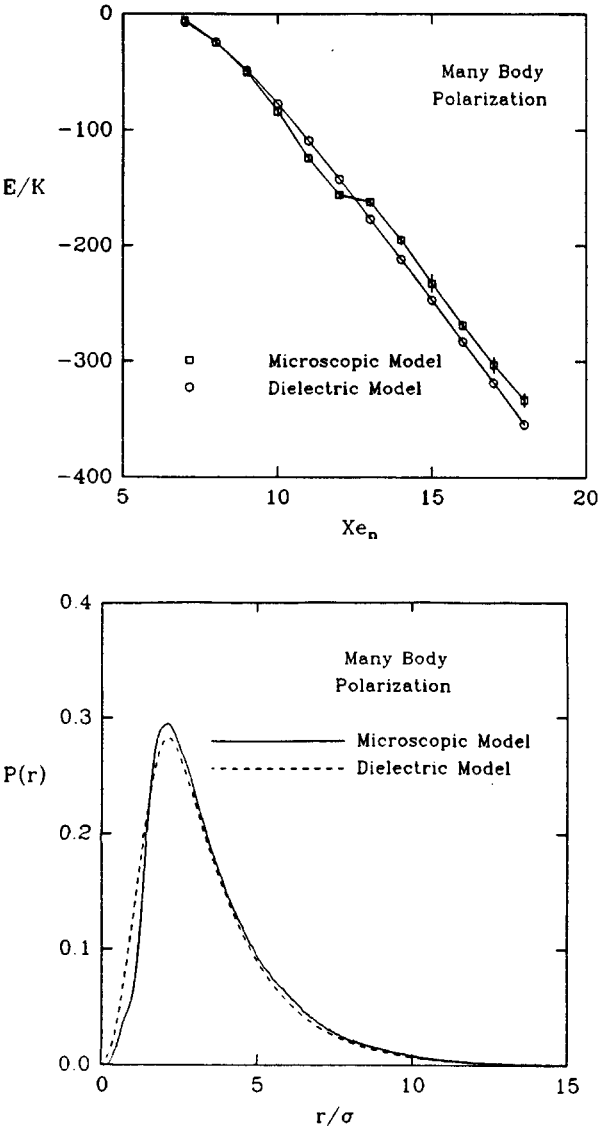

FIG. 10. The top figure shows a comparison of the ground state energy as of function of cluster size for the dielectric model and our microscopic model. The data for both models includes only pair polarization effects. The bottom figure shows the same comparison for the ground state wave function of Xe_{13}^-.

That is, we expanded Eq. (4.13) to first order in α. We again solved the radial Schrödinger equation for the resulting potential. Figure 11 shows the comparison of both the ground state energy as a function of cluster size and the ground state wave function of Xe_{13}^- for the two models. The agreement is poor for all cluster sizes indicating a break down of the theory. This implies that a dielectric model with no adjustable parameters cannot predict the observed scaling relation between the ground state energy calculated with pair polarization vs many-body polarization. If a value of $\rho = 0.011$ A^{-3} is chosen similar agreement similar to that found for many-body polarization is found at small cluster size $n \leqslant 15$ and the scaling is reproduced. However, at large cluster sizes the model breaks down as expected. In Fig. 11, the large shoulder in the wave function of the microscopic model can be clearly observed, a feature that cannot be reproduced by a continuum model. In total, these results suggest that in large

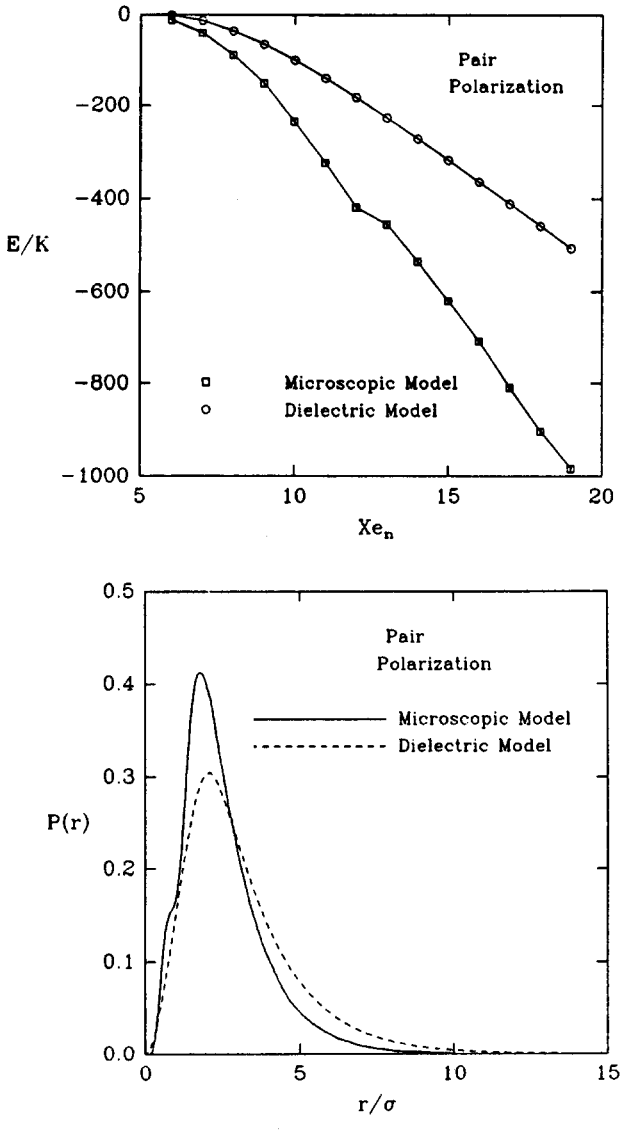

FIG. 11. The top figure shows a comparison of the ground state energy as of function of cluster size for the dielectric model and our microscopic model. The data for both models includes many-body polarization effects. The bottom figure shows the same comparison for the ground state wave function of Xe_{13}^-.

clusters the electron structure and binding energy should be sensitive to the microscopic features of the cluster thus precluding the validity of the continuum model. It may also indicate that the density is only a parameter in the theory which may be difficult to choose *a priori*. It should also be noted that the variational wave functions presented in this paper are based on the true cluster structure and are inexpensive to calculate. Therefore if one is interested in quick, reliable, approximate results for electron attachment to xenon clusters one should use a variational approach, rather than a continuum model.

The many-body polarization energy is much more expensive to calculate than the two-body polarization energy because it requires the solution of a system of linear equations [Eq. (2.4)]. It would be convenient if a renormalized pair polarization potential could be accurately defined to treat the many-body polarization terms. Lekner[24] has suggested a mean field approximation that can be used to determine such a potential. Briefly, consider the following form for the polarization potential:

$$V_p = \frac{-\alpha e^2 f(r) S^{1/2}(r)}{2r^4}, \tag{4.8}$$

where $S(r)$ is the switching function defined in Eq. (2.8). Now consider two xenon atoms a distance s apart, a distance r and t, respectively, from an electron. In this model the first xenon has an induced dipole moment, $\mathbf{p}$ along r of $\alpha e f(r) S^{1/2}(r)/r^2$ and the second has an induced dipole moment along t of $\alpha e f(t) S^{1/2}(t)/t^2$. The field along r due to the second atom maybe found from simple electrostatics[25]

$$\mathbf{E}(\mathbf{r})\cdot\hat{\mathbf{r}} = \frac{[3\hat{\mathbf{s}}(\mathbf{p}\cdot\hat{\mathbf{s}}) - \mathbf{p}]\cdot\hat{\mathbf{r}}}{s^3}, \tag{4.9}$$

$$\mathbf{E}(\mathbf{r})\cdot\hat{\mathbf{r}} = \frac{\alpha e S^{1/2}(t) f(t)}{2rs^3t^3} + \left[\frac{3(s^2+t^2-r^2)(s^2+r^2-t^2)}{2s^2} + (r^2+t^2-s^2)\right]. \tag{4.10}$$

Since the field along r is equal to the unscreened field plus the contribution due to all the other induced dipoles, if we integrate Eq. (4.10) times the probability of finding a neighbor a distance s away and add the unscreened field we have a self-consistent integral equation for $f(r)$. In a translationally invariant system the probability of finding an atom a distance s away is $\rho g(s) d\tau$. Therefore,

$$S^{1/2}(r) f(r) = S^{1/2}(r) - \pi\rho\alpha \int_0^\infty ds \frac{g(s)}{s^2} \int_{|r-s|}^{r+s} \times dt \frac{f(t) S^{1/2}(t)}{t^2} K(r,s,t),$$

$$K(r,s,t) = \frac{3(s^2+t^2-r^2)(s^2+r^2-t^2)}{2s^2} + (r^2+t^2-s^2). \tag{4.11}$$

This expression is not valid for a cluster. However, as

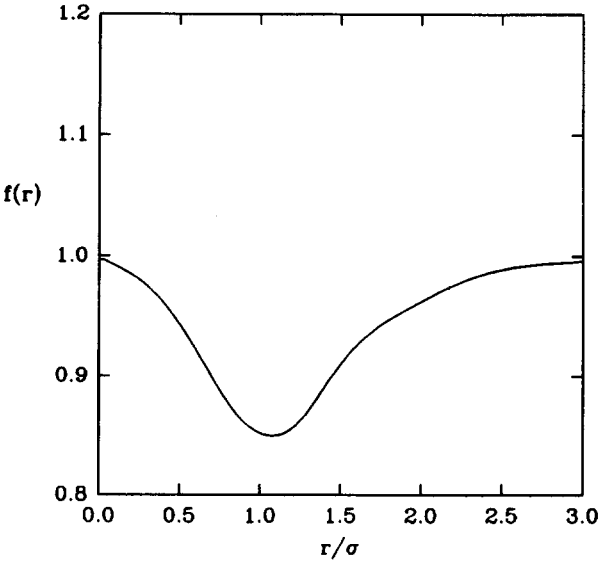

FIG. 12. The radial screening function which is postulated to reduce many-body polarization to an effective pair potential of the form of $\alpha e^2 f(r) S^{1/2}(r)/2r^4$.

$K(r,s,t)$ is proportional to $K(r,s,t) \sim 1/s^3$, the first neighbor peak is the most important and Eq. (4.11) might give a reasonable approximation. We therefore calculated the ground stte properties of the electron using the modified potential defined by Eqs. (4.8) and (4.11) for Xe_{13}^- [see Fig. 12 for $f(r)$]. The results were in reasonable agreement with those calculated using full many-body polarization ($E_0 \sim -155$ K vs $E_0 \sim -162$ K). This calculation indicates that a screening functions can be used to reduce many-body polarization to an effective pair potential.

ACKNOWLEDGMENTS

We would like to thank Professor David Coker and Professor Randall Dumont for many useful discussions during the course of this work. We would also like to thank Professor Stampfli and Professor Benneman for sending us a preprint of their work. This work was supported by a grant from NSF, and the simulations were run on the departmental Convex C2 computer.

[1]G. Martyna and B. J. Berne. J. Chem. Phys. **88**, 4516 (1988).
[2]D. F. Coker, D. Thirumali, and B. J. Berne. J. Chem. Phys. **86**, 5689 (1987).
[3]J. G. Gay and B. J. Berne. Phys. Rev. Lett **49**, 194 (1966).
[4]A. Wallqvist, G. Martyna, and B. J. Berne. J. Phys. Chem. **92**, 1721 (1988).
[5]A. Wallqvist, D. Thirumali, and B. J. Berne. J. Chem. Phys. **86**, 6404 (1986).
[6]M. R. Hoare and P. Pal. Adv. Phys. **20**, 161 (1971).
[7]M. R. Hoare and P. Pal. Adv. Phys. **24**, 646 (1975).
[8]P. Stampfli and K. Bennemann, Phys. Rev. A **71**, 1674 (1988).
[9]M. W. Cole and M. H. Cohen. Phys. Rev. Lett. **23**, 1238 (1969).
[10]J. A. Fleck, M. D. Feit, and A. Steiger. J. Comp. Phys. **47**, 412 (1982).
[11]R. Kosloff and D. Kosloff. J. Phys. Chem. **19**, 1823 (1983).
[12]J. Schnicker and P. J. Rossky. Phys. Rev. Lett **69**, 4628 (1988).
[13]F. H. Stillinger. J. Chem. Phys. **71**, 1674 (1979).
[14]J. A. Stratton, *Electromagnetic Theory* (McGraw–Hill, New York, 1941).
[15]R. C. Grimm and R. G. Storer. J. Comp. Phys. **7**, 134 (1971).
[16]J. B. Anderson. J. Chem. Phys. **63**, 4121 (1975).
[17]J. B. Anderson. Int. J. Quantum Chem. **15**, 109, (1979).
[18]J. B. Anderson. J. Chem. Phys. **73**, 3897 (1980).
[19]D. M. Ceperley and B. J. Alder. Phys. Rev. Lett. **45**, 566 (1980).
[20]J. B. Anderson, J. Chem. Phys. **82**, 2662 (1984).
[21]I. J. McGee and R. D. Murphy. J. Phys. C **5**, 311 (1972).
[22]D. J. Evans, Mol. Phys. **28**, 1233 (1974).
[23]B. R. Johnson, J. Chem. Phys. **67**, 4088 (1977).
[24]J. Lekner. Phys. Rev. **158**, 130 (1967).
[25]J. D. Jackson, *Classical Electrodynamics* (Wiley, New York, 1975).